Inorg. Chem. **2002**, *41*, 6358–6371

Mössbauer Study of Reduced Rubredoxin As Purified and in Whole Cells. Structural Correlation Analysis of Spin Hamiltonian Parameters

Vladislav V. Vrajmasu,[†] Emile L. Bominaar,[†] Jacques Meyer,[‡] and Eckard Münck*,[†]

Department of Chemistry, Carnegie Mellon University, 4400 Fifth Avenue, Pittsburgh, Pennsylvania 15213, and Département de Biologie Moléculaire et Structurale, CEA-Grenoble, 38054 Grenoble, France

Received August 9, 2002

The $[Fe^{II}(Cys)_4]^{2-}$ site of rubredoxin from *Clostridium pasteurianum* (Rd_{red}) has been studied by Mössbauer spectroscopy in both purified protein and whole cells of *Escherichia coli* overproducing it. Excellent fits were obtained to an $S = 2$ spin Hamiltonian for $D = 5.7(3)$ cm^{-1}, $E/D = 0.25(2)$, $\delta = 0.70(3)$ mm/s, $\Delta E_Q = -3.25(2)$ mm/s, $\eta = 0.75(5)$, $A_x = -20.1(7)$ MHz, $A_y = -11.3(2)$ MHz, and $A_z = -33.4(14)$ MHz. These parameters were analyzed with crystal-field theory for the ^{5}D manifold of iron(II), revealing a d(z^2) orbital ground state that is admixed by $\sim$0.21 d($x^2 - y^2$). The spin-Hamiltonian parameters are consistent within the ^{5}D theory, apart from the zero-field splitting parameter, D. This problem was solved by extending the crystal-field treatment with spin–orbit coupling to spin-triplet d–d excited states of the iron. Theoretical estimates are given for the spin-triplet (D_T) and spin-quintet contributions (D_Q) to D based on excitation energies derived from time-dependent density functional theory, TD-DFT. The computational results were interpreted in terms of crystal-field theory, yielding the Racah parameters $B = 682$ cm^{-1} and $C = 2583$ cm^{-1}. The theoretical analysis gives the relative magnitudes D_Q:D_T:$D_{ss} = 51\%$:42%:7% (D_{ss} originates from spin–spin interaction). The DFT analysis corroborates the pivotal role of the torsion angles (ω_i) of the C–S$_i$ bonds in shaping the electronic structure of the iron(II) site. Rd_{red} in overexpressing whole cells accounts for 60% of the Mössbauer absorption. The Rd_{red} spectra from whole cells are virtually identical to those of the purified protein. By using the theoretical ω dependence of the spin Hamiltonian parameters, the torsions for Rd_{red} in whole cells and purified protein samples are estimated to be the same within 2°. These findings establish Mössbauer spectroscopy as a structural tool for investigating iron sites in whole cells.

1. Introduction

Rubredoxins are small ($\approx$6 kDa, 55 amino acids) soluble proteins found in bacteria and archaea. The active site of rubredoxin (Rd) contains one iron atom, tetrahedrally coordinated to four cysteinyl residues, and can access the ferric (Rd_{ox}) and ferrous (Rd_{red}) oxidation states.[1] Although the rubredoxins have been structurally analyzed in considerable detail, only little information is available regarding their function.[1] These proteins are presently known to be involved as electron carriers in alkane hydroxylation in *Pseudomonas*.[2] Functions in iron metabolism and oxygen detoxification in sulfate-reducing bacteria[3] and in the assembly of photosystem II[4] have recently been proposed.

All aspects of Rd structure have been investigated in considerable detail in studies of the proteins and synthetic analogues of their metal sites. One of the most scrutinized Rd is that of *Clostridium pasteurianum* (*Cp*), which is the focus of the present paper. The available data include a 1.1 Å-resolution crystal structure of Rd_{ox},[5] as well as recently reported 1.5 Å-resolution structures of both Rd_{ox} and Rd_{red}, which were crystallized in their final oxidation state.[6] The data show an expansion of the average Fe−S bond length

* Author to whom correspondence should be addressed. E-mail: emunck@cmu.edu.
[†] Carnegie Mellon University.
[‡] CEA-Grenoble.

(1) Meyer, J.; Moulis, J.-M. In *Handbook of Metalloproteins*; Messerschmidt, A., Huber, R., Poulos, T., Wieghardt, K., Eds.; John Wiley and Sons: Chichester, U.K., 2001.
(2) van Beilen, J. B.; Neuenschwander, M.; Smits, T. H. M.; Roth, C.; Balada, S. B.; Witholt, B. *J. Bacteriol.* **2002**, *184*, 1722.
(3) da Costa, P. N.; Romao, C. V.; LeGall, J.; Xavier, A. V.; Melo, E.; Teixeira, M.; Saraiva, L. M. *Mol. Microbiol.* **2001**, *41*, 217.
(4) Wastl, J.; Duin, E. C.; Iuzzolino, L.; Dörner, W.; Link, T.; Hoffmann, S.; Sticht, H.; Dau, H.; Lingelbach, K.; Maier, U.-G. *J. Biol. Chem.* **2000**, *275*, 30058.
(5) Dauter, Z.; Wilson, K. S.; Sieker, L. C.; Moulis, J. M.; Meyer, J. *Proc. Natl. Acad. Sci. U.S.A.* **1996**, *93*, 8836.

10.1021/ic020508y CCC: $22.00
Published on Web 11/07/2002

by 0.10 Å upon reduction, which agrees well with the observations reported by Lane et al.[7] for the Rd analogue bis(*o*-xylyl-α,α′-dithiolato)ferrate. Crystal structures of other synthetic analogues of Rd_{ox} and Rd_{red} have been reported.[8−12]

Cp Rd has been thoroughly investigated with electronic absorption spectroscopy,[13,14] most recently by Yoo et al. who reported magnetic circular dichroism (MCD) studies of the wild type and two Cys → Ser mutants. Since Yoo et al. observed $E \rightarrow T_2$ d−d transitions at 5900 and 6300 cm^{-1}, a third transition between these manifolds would have to be below 3300 cm^{-1}. These transition energies depend on the tetrahedral splitting (10 Dq) as well as on axial and rhombic distortions of the E and T_2 manifolds. *Cp* Rd_{red} has been studied with Mössbauer spectroscopy by Schultz, Debrunner, and Winkler[15,16] who recorded data obtained in applied magnetic fields up to 2.4 T. At these comparatively weak fields, however, the expectation values of the electronic spin components, $-\langle S_{x,z}\rangle$, are substantially less than two and, consequently, the zero-field splitting parameter D and the x and z components of the ^{57}Fe magnetic hyperfine tensor cannot be accurately determined. To extract structural information from the spin Hamiltonian parameters, for instance by applying crystal-field theory,[17−19] the quantities D, A_x, and A_z have to be determined with higher precision than acquired in earlier reports.

Coucouvanis and co-workers have synthesized the model compound $[PPh_4]_2[Fe(SPh)_4]$ that has been shown by crystallography, electronic absorption spectroscopy, magnetic susceptibility, and Mössbauer spectroscopy to mimic the Fe site of Rd_{red} exceedingly well.[8] The axial ($D = 5.98$ cm^{-1}) and rhombic ($E = 1.42$ cm^{-1}) zero-field splitting (ZFS) parameters of the $S = 2$ ground multiplet of this complex have been determined by Champion and Sievers[20] with far-infrared magnetic resonance. More recently, Knapp et al.[21] have measured the g-values of this complex with high-frequency (94−371 GHz) EPR and obtained $g_x = g_y = 2.08$ and $g_z = 2.00$. Coucouvanis et al. observed a d−d band in the near IR at 5880 cm^{-1} and a shoulder at 7700 cm^{-1} in the electronic absorption spectrum of $[PPh_4]_2[Fe(SPh)_4]$ and assigned these features to $^5E \rightarrow {}^5T_2$ transitions in T_d symmetry.[8] Thus, there is now a complete set of spin Hamiltonian parameters and optical data available for assessing the electronic structure of this ferrous complex. Solomon and co-workers[11] have reported a comprehensive single-crystal MCD study of another model complex with tetrathiolate coordination, namely the $[Fe(SR)_4]^{2-}$ anion ($R = 2\text{-}(Ph)C_6H_4$). The structure of this model complex has strict S_4 symmetry, instead of the approximate D_{2d} symmetry of Rd_{red}, and stabilizes the $x^2 - y^2$ orbital ground state rather than a ground state of (approximate) z^2 symmetry, as observed for Rd_{red}. The study of $[Fe(S\text{-}2\text{-}(Ph)C_6H_4)_4]^{2-}$ revealed weak electronic absorption bands ($\epsilon < 10$ M^{-1} cm^{-1}) arising from spin-quintet to -triplet d−d transitions at energies ranging from ∼1.5 to 3 eV. These energies extended well below those of the spectral features in the Holm−Ibers complex $[Fe(S_2\text{-}o\text{-}xyl)_2]^{2-}$ that were assigned by Bair and Goddard[22] to these spin-forbidden transitions. Concomitantly, the zero-field splitting parameter for the ground state, arising from spin−orbit coupling with the spin-triplet states, was shown to be on the order of 1 cm^{-1}.

In the course of our recent investigation of two mutated forms of *C. pasteurianum* rubredoxin, C9S and C42S, with Mössbauer and MCD spectroscopy,[14] we have studied the wild-type protein in applied magnetic fields up to 8.0 T. The data, as reported here, have allowed us to determine D, A_x, and A_z with increased precision. The analysis carried out and reported here results in much better fits of the experimental data and thus provides a considerably improved description of the electronic and magnetic structure of the Rd_{red} metal site.

We have then addressed the fundamental question of the relationship between the spin Hamiltonian parameters and the geometry of the metal site. When this question is solved, structural data can be deduced from Mössbauer data when only the latter are available, as in whole-cell measurements (see below). To explore this possibility we have applied density functional theory (DFT) to a variety of isomers of a structural mimic for the metal center in Rd_{red} to obtain (the electronic distributions in) the ground states. These states were subsequently used for evaluating electronic properties, such as the electric field gradient at the iron nucleus, and as reference configurations for post-SCF calculations performed for the purpose of assessing the excited electronic states. The results from the latter were adopted as a starting point for calculations of the zero-field splittings in Rd_{red} and allowed us to give nonempirical estimates of the relative contributions to these quantities arising from spin−orbit coupling of the spin-quintet ground state with d → d spin-quintet and -triplet excited states.

Finally, we have proceeded to further validate in vivo Mössbauer spectroscopy that has proven to be a powerful method for the detection and analysis of iron sites in whole

(6) Min, T.; Ergenekan, C. E.; Eidsness, M. K.; Ichiye, T.; Kang, C. *Protein Sci.* **2001**, *10*, 613.
(7) Lane, R. W.; Ibers, J. A.; Frankel, R. B.; Papaefthymiou, G. C.; Holm, R. H. *J. Am. Chem. Soc.* **1977**, *99*, 84.
(8) Coucouvanis, D.; Swenson, D.; Baenziger, N. C.; Murphy, C.; Holah, D. G.; Sfarnas, N.; Simopoulos, A.; Kostikas, A. *J. Am. Chem. Soc.* **1981**, *103*, 3350.
(9) Millar, M.; Lee, J. F.; O'Sullivan, T.; Koch, S. A.; Fikar, R. *Inorg. Chim. Acta* **1996**, *243*, 333.
(10) Koch, S. A.; Maelia, L. E.; Millar, M. *J. Am. Chem. Soc.* **1983**, *105*, 5944.
(11) Gebhard, M. S.; Koch, S. A.; Millar, M.; Devlin, F. J.; Stephens, P. J.; Solomon, E. I. *J. Am. Chem. Soc.* **1991**, *113*, 1640.
(12) Gebhard, M. S.; Deaton, J. C.; Koch, S. A.; Millar, M.; Solomon, E. I. *J. Am. Chem. Soc.* **1990**, *112*, 2217.
(13) Eaton, W. A.; Palmer, G.; Fee, J. A.; Kimura, T.; Lovenberg, W. *Proc. Natl. Acad. Sci. U.S.A.* **1971**, *68*, 3015.
(14) Yoo, S. J.; Meyer, J.; Achim, C.; Peterson, J.; Hendrich, M. P.; Münck, E. *J. Biol. Inorg. Chem.* **2000**, *5*, 475.
(15) Schulz, C.; Debrunner, P. G. *J. Phys. Colloq.* **1976**, 153.
(16) Winkler, H.; Schulz, C.; Debrunner, P. G. *Phys. Lett. A* **1979**, *69A*, 360.
(17) Bertrand, P.; Gayda, J. P. *Biochim. Biophys. Acta* **1979**, *579*, 107.
(18) Bertrand, P.; Gayda, J. P. *Biochim. Biophys. Acta* **1988**, *954*, 347.
(19) Bertrand, P.; Guigliarelli, B.; Gayda, J. P.; Beardwood, P.; Gibson, J. F. *Biochim. Biophys. Acta* **1985**, *831*, 261.
(20) Champion, P. M.; Sievers, A. J. *J. Chem. Phys.* **1977**, *66*, 1819.
(21) Knapp, M. J.; Krzystek, J.; Brunel, L.-C.; Hendrickson, D. N. *Inorg. Chem.* **2000**, *39*, 281.
(22) Bair, R. A.; Goddard, W. A., III. *J. Am. Chem. Soc.* **1978**, *100*, 5669.

cells.[23] In our previous Mössbauer study of the FNR transcription factor, as purified and as overproduced in whole *Escherichia coli* cells, we observed background spectra arising from various iron-containing proteins and iron chelators. The background spectra exhibited relaxation effects at 4.2 K, which we ascribe to intermolecular spin−spin interactions. This observation suggested that the spectra of any paramagnetic protein might be distorted by spin−spin interactions with the paramagnetic neighbors in the cell. The well-characterized and well-resolved spectra of the paramagnetic Rd_{red} appeared to be ideally suited for an assessment of these phenomena. The spectra of Rd_{red} reported here, however, do not show any signs of intermolecular spin−spin interactions. Furthermore, the whole-cell spectra of Rd_{red} are virtually identical to those of the purified protein and indicate that the structures of Rd, as probed at the iron site, in whole cells and in the purified protein are essentially identical.

2. Materials and Methods

2.1. Protein Isolation and Whole-Cell Preparation. The preparation of ^{57}Fe-enriched *Cp* Rd has been described in detail.[24] In brief, *E. coli* cells, containing the *Cp* Rd-encoding plasmid, were grown in mineral medium (Na_2HPO_4, 6 g/L; KH_2PO_4, 3 g/L; NH_4-Cl, 1 g/L) supplemented with glucose (0.2%), $MgSO_4$ (1 mM), vitamin B_1 (0.5 mg/L), ampicillin (100 mg/L), kanamycin (50 mg/L), and ^{57}Fe (1 mg/L). Cells were harvested by centrifugation (30 min, 4500*g*), and *Cp* Rd was purified by several chromatographic steps as indicated.[24] The pure protein was reduced in an oxygen-free atmosphere by adding dithionite (0.2 M solution) to a final concentration 2−3-fold higher than the Rd concentration, transferred into a Mössbauer cell, and immediately frozen in liquid nitrogen. For the preparation of whole-cell Mössbauer samples, the culture conditions were slightly modified as follows. Only 20% of the final (1 mg/L) ^{57}Fe concentration was included in the culture medium, and the remainder was added upon induction[24] of the Rd gene expression. Cells were harvested by centrifugation (30 min, 4500*g*), resuspended in mineral medium (1/50 of the culture volume), and recentrifuged (30 min, 30 000*g*). The tight cell pellet thus obtained was packed into Mössbauer cells and immediately frozen at −80 °C. Mössbauer cells were filled with 700 ± 50 mg of cell pellet, which corresponded to ca. 0.35 L of culture. A control whole-cell sample was prepared by running a culture in the same conditions as described above with *E. coli* cells differing only by the absence of the *Cp* Rd-encoding plasmid.

2.2. Mössbauer Spectroscopy. Mössbauer spectra were collected on constant acceleration spectrometers, which allowed us to record spectra between 1.5 and 200 K in applied magnetic fields of up to 8.0 T. Isomer shifts are quoted relative to Fe metal at room temperature. The spectra were analyzed using the WMOSS software (WEB Research Co., Edina, MN).

2.3. DFT Calculations. Density functional calculations were performed using Becke's three-parameter hybrid functional (B3LYP) provided by the Gaussian 98W (release A.9) software package.[25] The basis set 6-311G of Pople and co-workers was used[26] unless otherwise stated. The electric field gradients (EFG) were also evaluated with Wachters (+f) all-electron basis set for iron,[27] while retaining the 6-311G basis set for the other atoms, and with the all-atom 6-311+G* basis set to improve the accuracy of electronic density on the metal ion.[26] Mulliken population analysis was used to monitor the electron distribution. The SCF calculations were terminated upon reaching tight convergence criteria (10^{-6} rmsd in the density matrix and 10^{-8} Hartree maximum deviation in energy). The calculations were performed on the truncated model $[Fe(SCH_3)_4]^{2-}$ of Rd_{red}. Geometries used were as follows: the X-ray structure of the iron−sulfur−carbon skeleton, an idealized D_{2d} structure based on averaged X-ray parameters, and a computationally optimized D_{2d} structure, which was subsequently distorted to C_2 symmetry to mimic the torsion S−Fe−S−C angles in Rd_{red}.

The energies of the Kohn−Sham orbitals failed to reproduce the observed excitation energies and are not presented. The energies of quintet → quintet d−d transitions were calculated by (i) time-dependent DFT (TD-DFT) and (ii) converging the SCF procedure in Kohn−Sham states of which the orbital populations were altered. The two methods result in excitation energies that are equal within the accuracy of the TD-DFT method implemented in Gaussian 98[28] (∼0.18 eV) and are in excellent agreement with experimental values (see Discussion). A number of orbital-nondegenerate, spin-uncontaminated triplet excited states were computed by altering the orbital occupations of the quintet ground state and converged to self-consistency. These states served as references for subsequent TD-DFT calculations from which additional triplet excitation energies were obtained. By analyzing the TD-DFT results, we were able to identify a part of the spin-triplet excitation scheme. As TD-DFT provides only linear combinations of singly substituted determinant wave functions, the remainder of the energies (necessary to compute the triplet contributions to the zero-field splitting) were derived by a crystal-field interpretation of the TD-DFT results.[29]

3. Results

Figures 1−3 and 4A show Mössbauer spectra of Rd_{red} from *Cp*. The spectra given in Figures 1 and 2 were recorded in magnetic fields applied parallel to the γ radiation. We have analyzed the spectra with the $S = 2$ spin Hamiltonian

$$\mathscr{H} = D\left[\hat{S}_z^2 - \frac{1}{3}S(S+1)\right] + E(\hat{S}_x^2 - \hat{S}_y^2) + \hat{\mathbf{S}}\cdot\mathbf{g}\cdot\mathbf{B} + \hat{\mathbf{S}}\cdot\mathbf{A}\cdot\hat{\mathbf{I}} - g_n\beta_n\hat{\mathbf{I}}\cdot\mathbf{B} + \mathscr{H}_Q \quad (1a)$$

$$\mathscr{H}_Q = \frac{eQV_{zz}}{12}[3\hat{I}_z^2 - I(I+1) + \eta(\hat{I}_x^2 - \hat{I}_y^2)] \quad (1b)$$

where D and E are the axial and rhombic ZFS parameters, respectively, **g** is the electronic **g**-tensor, **A** is the magnetic

(23) Popescu, C. V.; Bates, D. M.; Beinert, H.; Münck, E.; Kiley, P. J. *Proc. Natl. Acad. Sci. U.S.A.* **1998**, *95*, 13431.
(24) Meyer, J.; Gagnon, J.; Gaillard, J.; Lutz, M.; Achim, C.; Münck, E.; Petillot, Y.; Colangelo, C. M.; Scott, R. A. *Biochemistry* **1997**, *36*, 13374.
(25) Frisch, M. J.; Trucks, G. W.; Schlegel, H. B.; Scuseria, G. E.; Robb, M. A.; Cheeseman, J. R.; Zakrzewski, V. G.; Montgomery, J. A., Jr.; Stratmann, R. E.; Burant, J. C.; Dapprich, S.; Millam, J. M.; Daniels, A. D.; Kudin, K. N.; Strain, M. C.; Farkas, O.; Tomasi, J.; Barone, V.; Cossi, M.; Cammi, R.; Mennucci, B.; Pomelli, C.; Adamo, C.; Clifford, S.; Ochterski, J.; Petersson, G. A.; Ayala, P. Y.; Cui, Q.; Morokuma, K.; Malick, D. K.; Rabuck, A. D.; Raghavachari, K.; Foresman, J. B.; Cioslowski, J.; Ortiz, J. V.; Stefanov, B. B.; Liu, G.; Liashenko, A.; Piskorz, P.; Komaromi, I.; Gomperts, R.; Martin, R. L.; Fox, D. J.; Keith, T.; Al-Laham, M. A.; Peng, C. Y.; Nanayakkara, A.; Gonzalez, C.; Challacombe, M.; Gill, P. M. W.; Johnson, B. G.; Chen, W.; Wong, M. W.; Andres, J. L.; Head-Gordon, M.; Replogle, E. S.; Pople, J. A. *Gaussian 98*; Gaussian, Inc.: Pittsburgh, PA, 1998.
(26) Raghavachari, K.; Pople, J. A.; Replogle, E. S.; Head-Gordon, M. *J. Phys. Chem.* **1990**, *94*, 5579.

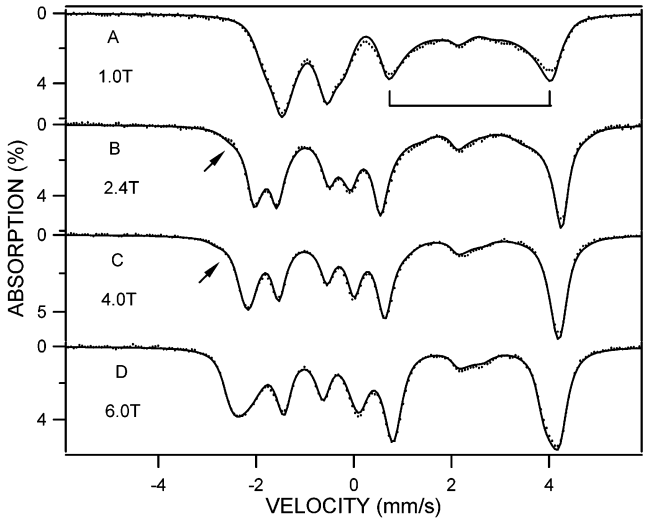

Figure 1. Mössbauer spectra of dithionite-reduced Rd from *Cp* recorded at 4.2 K in magnetic fields applied parallel to the γ rays. The solid lines are spectral simulations, using the parameters listed in Table 1. The bracket in the 1.0 T spectrum marks the splitting of the high-energy feature discussed in the text. Arrows mark the positions of the low-energy lines of the spectra associated with the first excited spin state; in zero applied field this state is 2.5 cm^{-1} above the ground state.

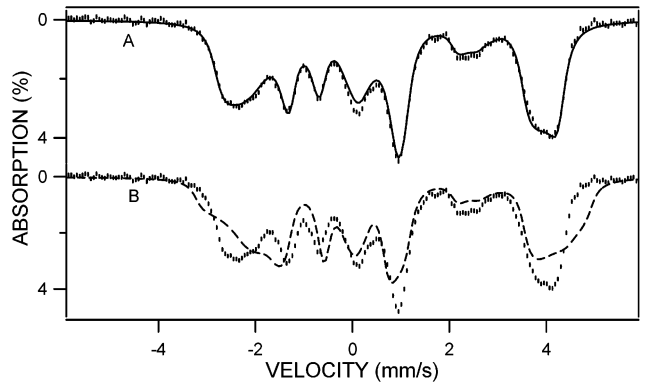

Figure 2. Spectrum of Rd_{red}, sample of Figure 1, recorded at 4.2 K in a parallel field of 8.0 T. The solid line in A is a theoretical curve generated with the parameters of Table 1. The dashed line in B is a theoretical spectrum generated with the previously published parameters.[15]

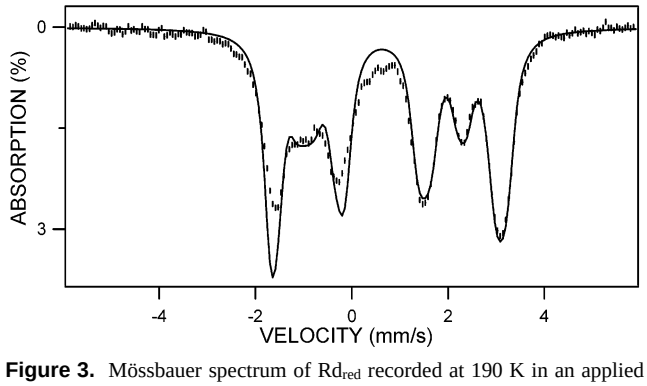

Figure 3. Mössbauer spectrum of Rd_{red} recorded at 190 K in an applied field of 8.0 T. The simulation (solid curve) has been performed in fast relaxation and describes the high-energy feature quite well but misses some of the low-energy features. The wings on the low-energy features indicate that the fast relaxation assumption is not quite fulfilled.

hyperfine tensor, and $\mathscr{H}_Q$ describes the interaction between the EFG, with tensor **V** and principal components V_{xx}, V_{yy},

(27) Wachters, A. J. H. *J. Chem. Phys.* **1970**, *52*, 1033.

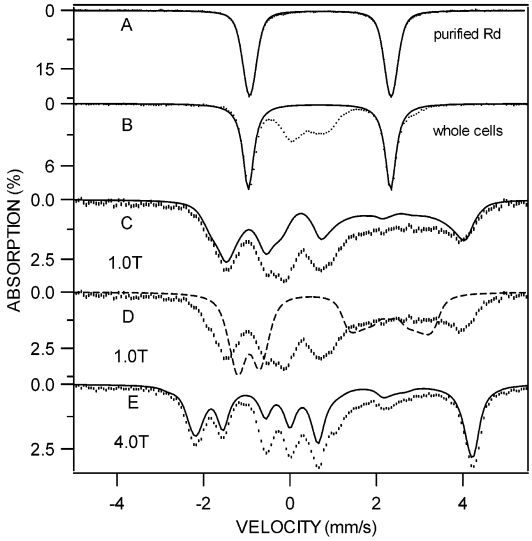

Figure 4. 4.2 K Mössbauer spectra of Rd_{red} as purified (A) and in whole *E. coli* cells (B−E) recorded in fields parallel to the γ radiation. The solid lines in B, C, and E are the spectra for the purified protein obtained under the same physical conditions. The dashed line D is a theoretical curve generated with the parameters of Table 1 in the limit of fast electronic spin relaxation.

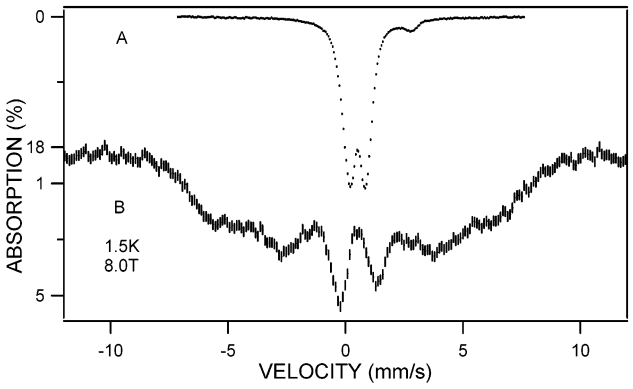

Figure 5. Mössbauer spectra of whole cells lacking Rd recorded at 4.2 K in zero field and at 1.5 K in a parallel field of 8.0 T.

and V_{zz}, and the nuclear quadrupole moment Q. $\eta = (V_{xx} - V_{yy})/V_{zz}$ is the asymmetry parameter; it is conventional to define the EFG tensor in a coordinate frame in which $|V_{zz}| \geq |V_{yy}| \geq |V_{xx}|$. We have investigated whether the EFG tensor is rotated relative to the principal axes of the ZFS and **A**-tensors. Our analysis did not provide any evidence for such rotations, and thus, we kept all tensors in the same principal axes frame for the final analysis. (The X-ray structure[6] suggests C_2 symmetry where the 2-fold y axis is one of the secondary axes of the idealized D_{2d} symmetry (called C_2' in Figure 6), implying that all tensors share a common principal axis along the symmetry axis. Thus, only rotations around this axis would be allowed.) The solid lines drawn through the spectra of Figures 1 and 2 are spectral simulations based on eq 1a,b, using the parameters listed in Table 1. A few comments regarding the simulations are in order.

(28) Wiberg, K. B.; Stratmann, R. E.; Frisch, M. J. *Chem. Phys. Lett.* **1998**, *297*, 60.
(29) Griffith, J. S. *The Theory of Transition-Metal Ions*; Cambridge University Press: London, 1961.

Table 1. 4.2 K Spin Hamiltonian Parameters of Rd_{red} and $[Fe(SPh)_4]^{2-}$

molecule	D cm^{-1}	E/D	δ mm/s	ΔE_Q mm/s	η	A_x MHz	A_y MHz	A_z MHz
$[Fe(SPh)_4]^{2-}$ [a]	+5.97[b]	0.24[b]	0.73(3)[c]	−3.24(3)	0.67	−20.5(4)	−11.2(3)	−34.2(3)
Cp Rd_{red}	+5.7(3)[c]	0.25(2)	0.70(2)	−3.25(2)	0.75(5)	−20.1(7)	−11.3(2)	−33.4(14)
calcd[d]	+3.92[d]	0.25		−3.25	0.75	−20.6	−11.4	−32.8

[a] For $[Fe(SPh)_4]^{2-}$ g-values are available from high-frequency EPR: $g_x = g_y = 2.08$, $g_z = 2.00$. [b] Zero-field splitting parameters from far-infrared study of Champion and Sievers.[20] [c] Numbers in parentheses give estimated uncertainties in last significant digits. [d] Using expressions given by Bertrand and Gayda.[17−19] Accurate calculation of D requires consideration of triplet states (see text).

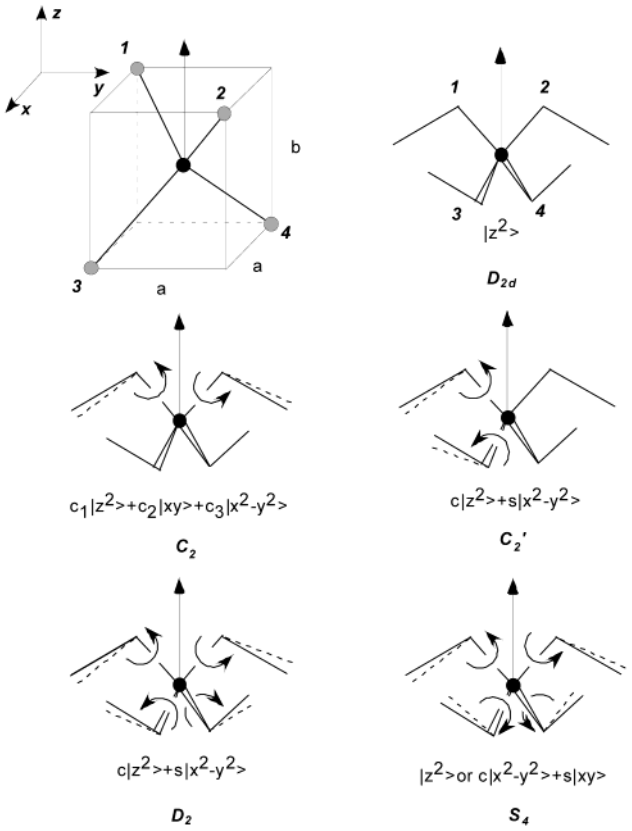

Figure 6. Structural parameters relevant for the idealized distortions in the coordination shell of iron in Rd and synthetic analogues (top left). Schematic representations of structures and their idealized symmetries of the $[Fe(SC)_4]$ units in Rd and synthetic analogues that are used in theoretical analyses. Allowed mixings of d orbitals z^2, $x^2 - y^2$, and xy are indicated for each symmetry, with orbitals defined in Cartesian frame at top, left. Vertical arrows are the S_4 axis of the double-bird structure at top, right; the C_2' axis is along y, bisects the angle S_1-Fe-S_3, and is perpendicular to the S_4 (z) axis. The $[Fe(SC)_4]$ units and axes have been rotated by 45° around the S_4 axis relative the top left diagram for presentational purposes.

The high-energy features of the low-field spectra depend primarily on A_y and $\langle S_y \rangle$, the expectation value of the y component of the electronic spin for the lowest state; for $D > 0$ this state is the $M_S = 0$ state in the limit of axial symmetry. The splitting of this high-energy feature, indicated by the bracket in the 1.0 T spectrum, depends primarily on A_y, D, and E/D. By following the splitting of this feature as a function of the applied field we were able to constrain the range of these parameters to $A_y = -11.3 \pm 0.2$ MHz, $D = 5.7 \pm 0.3$ cm^{-1}, and $E/D = 0.25 \pm 0.02$. Computation of the $\langle S_i \rangle$ for the first excited spin level (the $M_S = -1$ state) shows that $\langle S_z \rangle$ has the largest magnitude. This state is partially populated at 4.2 K, and since the electronic relaxation is slow at 4.2 K, this state produces its own Mössbauer spectrum. The left-most feature of the spectrum associated with this excited state is a measure of A_z and appears as a shoulder (arrow) in the 2.4 and 4.0 T spectra. A_x is most precisely determined in strong applied fields. For $B > 4.0$ T the expectation value $\langle S_x \rangle$ has sufficient magnitude to produce a sizable internal field, $B_{int,x} = -\langle S_x \rangle A_x / g_n \beta_n$ along x. $B_{int,x}$ determines the splitting pattern of the four low-energy lines in Figures 1C,D and 2A. Finally, the distinct triplet pattern of the high-energy feature of the 190 K spectrum of Figure 3 determines that $\Delta E_Q < 0$ and $\eta \approx 0.7$. Previous studies by Winkler et al.[16] revealed that the electronic spin of Rd_{red} is not yet in the fast relaxation regime even at 150 K, a circumstance that hampers the determination of the spin Hamiltonian parameters. This is also true at 190 K, although the problem is less severe in strong applied fields. The high-field feature of the 190 K spectrum can be simulated very well by assuming the fast fluctuation limit. It can be seen, however, that the low-energy features exhibit some broad wings, indicating intermediate relaxation for some molecular orientations.

After having obtained good simulations for the individual spectra, on the basis of considerations outlined above, we have fitted simultaneously groups of four spectra. Overall, the fits of the 4.2 K spectra are of very good quality and allowed an accurate determination of all parameters in Table 1. For comparison we show in Figure 2B a spectral simulation of the 8.0 T spectrum (dashed), using the previously published parameters[15] that were obtained in applied fields smaller than 2.5 T. While these parameters fit the low-field spectra quite well (see Figure 3C of Schultz and Debrunner[15]), determination of D and A_x requires the application of strong magnetic fields.

To assess the energy of the lowest excited orbital state of Rd_{red} we have analyzed the temperature dependence of the Mössbauer spectra recorded in zero magnetic field and obtained for ΔE_Q in mm/s (±0.02 mm/s) the series 3.25 (40 K), 3.23 (90 K), 3.23 (120 K), 3.21 (180 K), 3.20 (210 K), and 3.20 (225 K). In principle, the temperature dependence of ΔE_Q can be utilized to determine the energy of low-lying orbital states.[30] However, the effect in Rd_{red} is so weak that the population of vibrational levels, rather than the population of orbital states, could be the determining factor. Therefore, we have not attempted to derive a value for the lowest orbital excitation energy from these variable-temperature data but instead estimated a lower limit for this energy, 600 cm^{-1}.

(30) Johnson, D. P.; Ingalls, R. L. *Phys. Rev. B* **1970**, *1*(3), 1013.

Figure 4B,C,E shows 4.2 K Mössbauer spectra obtained from whole *E. coli* cells that overproduce *Cp* Rd (Materials and Methods). The most prominent feature of the zero-field spectrum of Figure 4B is a quadrupole doublet (representing ca. 60% of total ^{57}Fe) with parameters identical to those of the purified Rd_{red} (see Figure 4A). This doublet is readily distinguished from those of octahedral ferrous sites with O/N coordination by its characteristic isomer shift ($\delta = 0.70$ mm/s as compared to $\delta \approx 1.2-1.3$ mm/s for $Fe^{II}X_{5-6}$, X = N or O). The small shoulder on the high-energy line of the Rd doublet originates most likely from a small amount (<5% of total iron) of high-spin Fe^{II} with $\delta = 1.2-1.3$ mm/s. The feature seen in the central portion of the spectrum represents iron-containing species other than Rd. These species seem (see below) to be present also in the control of Figure 5A obtained with cells not containing the Rd gene. We do not know which proteins or iron complexes contribute to the absorption of the control or to the absorption in the central part of Figure 4B, but the high-field spectra indicate that most of this absorption belongs to high-spin ferric species.

Figure 4C,E shows spectra of the Rd-overproducing cells recorded in parallel fields of 1.0 and 4.0 T, respectively. The solid lines drawn through the data are the theoretical curves of Figure 1A,C, plotted to represent 60% of the Fe. It can be seen that the spectra of the purified protein almost exactly match those observed in the whole *E. coli* cells. Most interestingly, the Rd_{red} spectrum of the whole cells is observed in the limit where the electronic spin relaxes slowly on the Mössbauer time scale (i.e., slowly as compared to 10 MHz), which answers the question posed in the Introduction. To illustrate this point, we show in Figure 4D (same data as in Figure 4C) a theoretical spectrum (dashed) calculated assuming fast electronic spin fluctuation.

4. Discussion

In section 4.1 we interpret the spin Hamiltonian parameters obtained for Rd_{red} in the framework of crystal-field theory. In section 4.2 the structure dependencies of the zero-field splittings and the spatially anisotropic hyperfine interactions are analyzed by means of DFT calculations. Special attention is paid to the spin-triplet contributions to zero-field splitting parameters. Finally, the relationships established between the electronic and geometrical structures are used in section 4.3 as an analytical tool for comparing the active-site structures of Rd_{red} in whole cells and purified protein samples.

4.1. Crystal-Field Analysis of Spin Hamiltonian Parameters of Rd_{red}. Expressions for the spin-quintet contributions to the hyperfine parameters for a high-spin Fe^{2+} site in a D_2 distorted tetrahedral crystal field have been given by Bertrand and Gayda.[17-19] In this symmetry the $|x^2 - y^2\rangle$ and $|z^2\rangle$ states of the e-manifold in T_d are allowed to mix and yield the ground state

$$|\varphi\rangle \approx \cos\theta|z^2\rangle + \sin\theta|x^2 - y^2\rangle \tag{2}$$

where θ is a mixing parameter that is related to the torsion angles $S'-Fe-S-C_\beta$ (see below). The hyperfine parameters are functions of θ and the orbital energies, ϵ_i. The magnetic hyperfine parameters are given by[17]

$$A_x = -P\left[\kappa - \frac{1}{7}\left(2\sin^2\left(\theta + \frac{\pi}{3}\right) - 1\right) - \frac{2\zeta}{\epsilon_{yz}}\sin^2\left(\theta + \frac{\pi}{3}\right)\right] \tag{3a}$$

$$A_y = -P\left[\kappa - \frac{1}{7}\left(2\sin^2\left(\theta - \frac{\pi}{3}\right) - 1\right) - \frac{2\zeta}{\epsilon_{xz}}\sin^2\left(\theta - \frac{\pi}{3}\right)\right] \tag{3b}$$

$$A_z = -P\left[\kappa - \frac{1}{7}(2\sin^2\theta - 1) - \frac{2\zeta}{\epsilon_{xy}}\sin^2\theta\right] \tag{3c}$$

and the electric hyperfine parameters read as

$$\Delta E_Q = \frac{1}{2}eQV_{zz}\sqrt{1 + \frac{1}{3}\eta^2} \tag{4a}$$

$$\eta = \frac{V_{xx} - V_{yy}}{V_{zz}} = -\sqrt{3}\tan 2\theta \tag{4b}$$

Equation 3 includes the Fermi contact term ($\sim\kappa$), the spin dipolar coupling ($\sim 1/7$), which is traceless, and the orbital term ($\sim\zeta/\epsilon$, where ζ is the one-electron spin−orbit coupling constant of iron); $P = 2g_n\beta_n\langle r^{-3}\rangle$ is a scaling factor. Equation 4a presents the quadrupole splitting, and eq 4b gives the asymmetry parameter. Although the actual C_2 symmetry in Rd_{red} is lower than D_2 and allows interaction between the *xz* orbital and the ground state, the ensuing admixture and changes in the hyperfine parameters are small because of the large energy gap, separating this orbital state from the ground state. These expressions are complemented by those for the *g*-values and zero-field splitting parameters given by Abragam and Bleaney[31]

$$g_x - g_e = \frac{2\zeta}{\epsilon_{yz}}\sin^2\left(\theta + \frac{\pi}{3}\right) \tag{5a}$$

$$g_y - g_e = \frac{2\zeta}{\epsilon_{xz}}\sin^2\left(\theta - \frac{\pi}{3}\right) \tag{5b}$$

$$g_z - g_e = \frac{2\zeta}{\epsilon_{xy}}\sin^2\theta \tag{5c}$$

where g_e is the *g* value for the free electron, and

$$D = 3\left(\rho + \frac{\zeta^2}{16\epsilon}\right)\cos 2\theta \tag{6a}$$

$$\frac{E}{D} \approx -\frac{1}{\sqrt{3}}\tan 2\theta \tag{6b}$$

where ρ is the spin−spin coupling constant for the 3d electrons of iron. In eq 6a,b the 3d orbitals of t_2 parentage in T_d are assumed to be degenerate, $\epsilon = \epsilon_{xy} = \epsilon_{yz} = \epsilon_{xz}$. As we shall show in section 4.2, this assumption does not hold in Rd_{red}. However, because it has been realized for quite some time[15] that the orbital ground state of Rd_{red} has predominantly z^2 symmetry ($\theta \approx 0$), eq 6a may still be applied, provided ϵ is identified with the energies of the quintet states *xz* and *yz* that interact with the ground state. (N.B. There is no spin−

(31) Abragam, A.; Bleaney, B. *Electron Paramagnetic Resonance of Transition Ions*; Oxford University Press: New York, 1970.

orbit coupling between z^2 and xy because of the selection rule $\Delta M_L = 0, \pm 1$.)

The expressions in eqs 3−5 depend on eight theoretical parameters: θ, V_{zz}, P, κ, ζ, ϵ_{xz}, ϵ_{yz}, and ϵ_{xy}. Ten related observables have been determined for Rd_{red}: ΔE_Q, η, A_x, A_y, and A_z by Mössbauer spectroscopy; ϵ_{xz} and ϵ_{yz} by MCD; and Δg_x, Δg_y, and Δg_z by EPR of $[Fe(SPh)_4]^{2-}$. The experimental value for η gives $\theta = -11.8°$ (eq 4b); ΔE_Q yields V_{zz} for a given value of η (eq 4b), and $\epsilon_{xz} = 5900$ cm^{-1} and $\epsilon_{yz} = 6300$ cm^{-1} have been measured directly by MCD.[14] $\Delta g_z \approx 0$ because θ is small (eq 5c), and therefore, ϵ_{xy} cannot be assessed by this analysis. There remain three unknowns (P, κ, ζ) for fitting five observables (A_x, A_y, A_z, Δg_x, Δg_y). (N.B. The values for Δg_x and Δg_y in Rd_{red} have not been determined, and we have adopted the results for $[Fe(SPh)_4]^{2-}$.) If eqs 3−5 are realistic, it must be possible to find acceptable values for the three unknowns that reproduce the five observables; if not, discrepancies between the results of eqs 3−5 and the observed values are expected for any values of P, κ, and ζ. By minimizing the discrepancies in a stepwise manner we obtained the values $P = 63.0$ MHz, $\kappa = 0.40$, and $\zeta = 350 \pm 20$ cm^{-1}, which are consistent with the results of earlier studies.[31] Substitution of the values obtained for the eight theoretical quantities in eqs 3−5 generates the spin Hamiltonian parameters listed in the third row of Table 1. All parameters are reproduced very well and support the validity of eqs 3−5. The calculated g-values, $g_x = 2.07$, $g_y = 2.11$, $g_z = 2.00$, and $g_{av} = 2.067$, match within the uncertainties the g-values reported by Knapp et al.[21] for $[Fe(SPh)_4]^{2-}$, namely, $g_x = g_y = 2.08 \pm 0.04$ and $g_z = 2.02 \pm 0.04$. By taking the trace of the experimental **A**-tensor we obtain $A_{iso} = -21.6$ MHz. This quantity contains contributions from the Fermi contact term, $A_{contact}$, and the (orbital) pseudo-contact interaction, $A_{pseudo} = P(\mathrm{Tr}(\mathbf{g} - 2))/3$. By using the calculated g-values we obtain for Rd_{red} the value $A_{pseudo} = +4.2$ MHz and $A_{contact} = A_{iso} - A_{pseudo} = -25.8$ MHz. By removing A_{iso} and the anisotropic part of the orbital term, $P(g_i - g_{av})$, from the **A**-tensor components we obtain the spin-dipolar contribution to the **A**-tensor, $A_x^{sd} = +0.8$ MHz, $A_y^{sd} = 7.5$ MHz, and $A_z^{sd} = -8.3$ MHz. The parameters evaluated here are important for the analysis of spin-coupling schemes for iron−sulfur clusters; for details the reader is referred to Mouesca and co-workers.[32] The components of the valence part of the EFG tensor are proportional to those of $\mathbf{A}^{sd}$ (eq 19.32 of ref 31). The anisotropy $\eta_{sd} = (A_x^{sd} - A_y^{sd})/A_z^{sd} = 0.81$ matches quite well the experimental asymmetry parameter of the EFG, $\eta = (V_{xx} - V_{yy})/V_{zz} = 0.75(5)$, confirming that the EFG tensor of Rd_{red} is dominated by the valence contribution.

The values for ζ (350 cm^{-1}) and $\epsilon \approx \epsilon_{xz} \approx \epsilon_{yz}$ (~6100 cm^{-1}) given above can be used for estimating D. Substitution of these parameter values in eq 6a gives $D = 3.3 \pm 0.5$ cm^{-1}, which is significantly lower than the experimental value of 5.7 cm^{-1}. Two alternative explanations for the discrepancy have emerged from the literature. On the basis of eq 6a and literature values for ζ and ϵ, Knapp et al.[21] estimated a value similar to ours (~3 cm^{-1}) for D in the Rd_{red} model $[Fe(SPh)_4]^{2-}$ ($D_{exp} = 5.7$ cm^{-1}) and ascribed the missing zero-field splitting (+2.7 cm^{-1}) to spin−spin coupling. Alternatively, Gebhard et al.[11] reported a spin-triplet contribution to the negative zero-field splitting in the synthetic complex $[Fe(S\text{-}2\text{-}(Ph)C_6H_4)_4]^{2-}$ ($D_{exp} = -8.7$ cm^{-1}) of about −1.2 cm^{-1}, suggesting triplet contributions to D as a possible source for the discrepancy between the experimental and the eq 6a-based values for this parameter in Rd_{red}. The two contributions to D in Rd_{red} are discussed in section 4.2.

4.2. DFT Calculations of the Fine Structure and Electric Hyperfine Interactions. The 3d levels of iron(II) split in a crystal field of tetrahedral symmetry (T_d) into the degenerate sets $e = \{z^2, x^2 - y^2\}$ (lowest) and $t_2 = \{xy, yz, xz\}$, where the orbitals are defined in the Cartesian coordinates of Figure 6. Distortions from T_d may further lower the degeneracy and stabilize a nondegenerate ground state. The electric field gradient indicates the energy order in which the e components appear: ΔE_Q is positive or negative depending on whether the ground state is $x^2 - y^2$ or z^2, respectively. A positive sign has been predicted for $[Fe(S\text{-}2\text{-}(Ph)C_6H_4)_4]^{2-}$ based on the $x^2 - y^2$ ground state deduced from MCD analysis (however, a Mössbauer proof of this property is lacking), and negative signs have been inferred from the Mössbauer spectra of Rd_{red}, $[Fe(SPh)_4]^{2-}$, and $[Fe(S_2\text{-}o\text{-}xyl)_2]^{2-}$. The distortions in the coordination shell of iron are easily visualized by inscribing the structure in a cube (Figure 6). In T_d the edges, a and b, are equal, and the bond angles at iron, $\alpha_{ij} = S_i\text{−}Fe\text{−}S_j$ are 109.5°. The edges of the cube differ in D_{2d}, $a \neq b$, and the angles assume two values, $\alpha = \alpha_{12} = \alpha_{34}$ and $\alpha' = \alpha_{13} = \alpha_{14} = \alpha_{23} = \alpha_{24}$. The D_{2d} structure is called elongated when $a < b$ and $\alpha < \alpha'$ (two smaller angles and four larger ones). In the extreme case ($a = 0$, $b = 2$ Fe−S, $\alpha = 0$, and $\alpha' = 180°$) the ligands are in axial positions and, obviously, raise the z^2 orbital in energy (elongation → $x^2 - y^2$ ground state). The structure is called compressed when $a > b$ and $\alpha > \alpha'$ (four smaller angles and two larger ones). In the extreme case ($a = 2^{1/2}$ Fe−S, $b = 0$, $\alpha = 180°$, and $\alpha' = 90°$) the ligands occupy equatorial positions in which they raise the $x^2 - y^2$ orbital in energy (compression → z^2 ground state). Unfortunately, the two geometries have been confused by several authors,[8,21] which has led to erroneous conclusions about the origin of the crystal-field splittings in Rd. Given that the coordination spheres in Rd_{red} and $[Fe(SPh)_4]^{2-}$ are elongated (see Table 2), one predicts (on the basis of crystal-field theory) that $\Delta E_Q > 0$ (however, observed is $\Delta E_Q < 0$ in both systems). Analogously, the compressed coordination sphere in $[Fe(S\text{-}2\text{-}(Ph)C_6H_4)_4]^{2-}$ would imply $\Delta E_Q < 0$ (the ground state inferred from MCD suggests $\Delta E_Q > 0$). Thus, the crystal-field splittings of the e manifold predicted by crystal-field theory are at variance with those inferred from the spectroscopic data of a number of systems. The failure to explain the e-splittings on the basis of distortions in the first coordination shell suggests the application of theories that can describe the influence of the second nearest neighbors on the 3d-orbital energies. As pointed out by Bair and

(32) Mouesca, J. M.; Noodleman, L.; Case, D. A.; Lamotte, B. *Inorg. Chem.* **1995**, *34*, 4347.

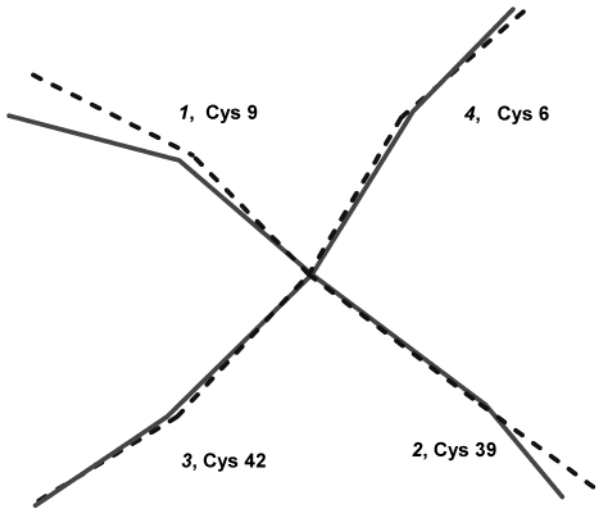

Figure 7. Overlay of $[Fe(SC)_4]$ units in Rd_{red} and $[PPh_4]_2[Fe(SPh)_4]$ showing the similarity in the torsion angles ω in these species.

Goddard,[22] the orientation of the $C_\beta-S$ bond, defined by the torsion angles ω_i in Figure 6 ($\omega_i = C-S-Fe-S'$), directs the lone pairs at sulfur and thereby affects the energies of the 3d orbitals. To corroborate this point, the latter authors performed a large scale ab initio calculation on the structure of the Holm−Ibers complex, $[Fe(S_2\text{-}o\text{-}xyl)_2]^{2-}$, and obtained a ground state of approximately z^2 symmetry, in agreement with the Mössbauer data. We note that the z^2 (A_1) and $x^2 - y^2$ (B_1) orbitals in the Holm−Ibers complex do not mix because they belong to different irreducible representations of the idealized D_{2d} symmetry in the $[Fe(SC)_4]$ core of this system; the allowed linear combinations of z^2, $x^2 - y^2$ (e) and xy (t_2) in the ground state have been summarized in Figure 6 for several symmetries. Ueyama et al. analyzed[33] the ω_i dependence of the 3d energies in Rd_{ox} with IEHT and obtained z^2 as the lowest 3d orbital at torsion angles of the observed magnitude. However, the C_2 symmetry adopted by these authors differs from the C_2'-like symmetry of the iron site in Rd (see below). The unit $[Fe(SCH_3)_4]^{2-}$ attains its highest, D_{2d}, symmetry in the double-bird arrangement ($\omega_i = 0$ for $i = 1-4$) shown in Figure 6, in which the birds are interchangeable by an S_4 operation (the S_4 axis is depicted by a vertical arrow). (N.B. There is a second D_{2d} conformation ($\omega_i = 180°$ for $i = 1-4$), which is approximately found in the $[Fe(SC)_4]^{2-}$ core of the Holm−Ibers complex.) Although the X-ray structure for the $[Fe(SC_\beta)_4]$ unit in Rd_{red} resembles the double-bird conformation, a closer examination shows a symmetry lower than D_{2d}. A view of the central units in Rd_{red} and the synthetic model $[Fe(SPh)_4]^{2-}$ along the S_4 axis of the idealized D_{2d} symmetry reveals torsion angles $\omega_1 \approx \omega_3 > 0$ and $\omega_2 \approx \omega_4 \approx 0$ (Figure 7) that are compatible with an approximate C_2' symmetry. (See Figure 6; the prime has been introduced to distinguish the C_2 axis perpendicular to S_4 from the parallel C_2 axis. The C_2' operation on the active site in Rd_{red} relates Cys9 to Cys42 and Cys6 to Cys39, and 2-fold rotation about S_4 transforms Cys6 to Cys42 and Cys9 to Cys39.[1]) The structural comparison given in Figure 7 suggests that the virtual identity of the fine-structure and hyperfine parameters in the two depicted species (Table 1) originate from an accidental coincidence of the key parameters, ω_i. We have analyzed the influence of these structural features on the orbital ground state and its properties by applying DFT. The calculations were performed on the model $[Fe(SCH_3)_4]^{2-}$ in various conformations. The calculation on the D_{2d} structure (Figure 6), constructed by averaging the bond distances and angles in the crystal structure of Rd_{red} from *Cp* (Table 2) and taking $\omega_i = 0$, resulted in a d^6 ground state in which the z^2 orbital is doubly occupied (i.e., the β-HOMO is z^2), in agreement with earlier X_α results.[34] In contrast to their mixing properties in D_{2d} (see above), the orbitals z^2 (A) and $x^2 - y^2$ (A) do mix in C_2' symmetry. The DFT calculations in this symmetry were performed on structures in which the initial D_{2d} geometry was distorted by rotating one thiolate group in each bird, $\omega = \omega_1 = \omega_3 \neq 0$ (Figure 6), where a positive (counterclockwise) torsion angle, as observed in Rd_{red}, corresponds to a shortening of the C_1-C_3 distance. The orbital function of β-HOMO obtained in the DFT calculations can be approximated by the expression in eq 2, in which $\theta = 0$ for D_{2d}. The orbital calculated for Rd_{red} is depicted in Figure 8 and has lobes that are aligned along the x, y, and z axes, defined in Figure 6. These axes coincide with the principal axes of the EFG, and the orbital amplitudes along these directions are a measure for the corresponding components of the EFG tensor. The DFT results for the β-HOMO, acquired by scanning the geometry of the C_2' isomer, show a linear increase in the coefficient of $x^2 - y^2$ as a function of ω, provided the rotations are small. Thus, the DFT mixing angle, θ, is calculated to be proportional to the torsion, $\theta \approx -0.65\ \omega$, in the small angle approximation $\sin\theta \approx \theta$. The DFT value for the quadrupole splitting, ΔE_Q, is about −3.5 mm/s in D_{2d} (see below) and remains virtually constant along the C_2' coordinate, ω. In contrast, the DFT values of the rhombicity parameter, η, represent a nearly

Table 2. Structure Parameters for Rd_{red} and $[Fe(SPh)_4]^{2-}$

	Cp Rd_{red}[a]		$[Fe(SPh)_4]^{2-}$ [b]	
geometric param.	value[c]	average	value[c]	average
Fe−S1	2.369		2.335	
Fe−S2	2.394	2.363	2.355	2.352
Fe−S3	2.306		2.359	
Fe−S4	2.384		2.360	
Fe−S1−C1	105.0		110.4	
Fe−S2−C2	97.1	103.1	109.2	110.9
Fe−S3−C3	112.0		114.1	
Fe−S4−C4	98.3		109.8	
S1−Fe−S2	103.9		101.3	
S1−Fe−S3	110.1		119.0	
S1−Fe−S4	112.3	104.7 (1−2, 3−4)	111.5	99.6 (1−2, 3−4)
S2−Fe−S3	112.5	111.9	112.7	114.6
S2−Fe−S4	112.8		115.3	
S3−Fe−S4	105.5		97.9	
S1−Fe−S2−C2	−5.6	−3.9	6.6	7.6
S2−Fe−S1−C1	20.9	(1−2−2, 3−4−4)	11.5	(1−2−2, 3−4−4)
S3−Fe−S4−C4	−2.1	20.5	8.5	11.8
S4−Fe−S3−C3	20.1	(2−1−1, 4−3−3)	25.1	(2−1−1, 4−3−3)

[a] Ref 6. [b] Ref 8. [c] Distances in Å; angles in degrees.

(33) Ueyama, N.; Sugawara, T.; Tatsumi, K.; Nakamura, A. *Inorg. Chem.* **1987**, *26*, 1978.

(34) Noodleman, L.; Norman, J. G., Jr.; Osborne, J. H.; Aizman, A.; Case, D. A. *J. Am. Chem. Soc.* **1985**, *107*, 3418.

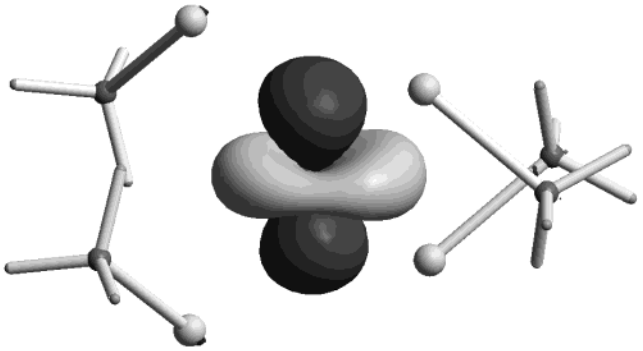

Figure 8. Contour plot of β-HOMO calculated by DFT in an idealized, C_2'-distorted $[Fe(SCH_3)_4]^{2-}$ model that mimics the central unit in Rd_{red}. $\omega \approx 20°$; other bond angles and distances were taken as in the D_{2d}-averaged X-ray structure of Rd_{red}.

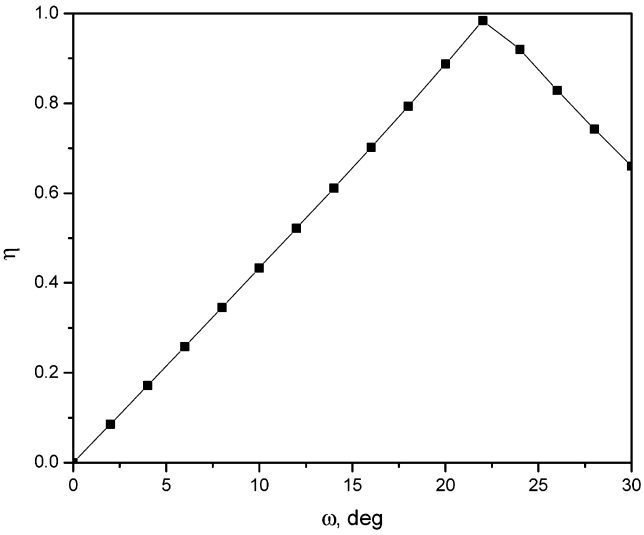

Figure 9. Asymmetry parameter η vs C_2' distortion angle ω calulated by DFT. Bond angles and distances were taken as in the D_{2d}-averaged X-ray structure of Rd_{red}.

linear function of ω (see Figure 9). (N.B. The corner in the η vs ω curve of Figure 9 is due to the convention $|\eta| \leq 1$ and reflects a change in the order of $|V_x|$, $|V_y|$, and $|V_z|$.) The computed η values are accurately described by the valence-only expression (eq 4b) for this quantity in the state of eq 2, from which one derives a linear function of the torsion

$$\eta(\omega) \approx \sqrt{3}\tan(1.3\omega) \approx 2.3\omega \qquad (7)$$

in the small angle approximation. The expression for V_{zz} in the state of eq 4a is $V_{zz}^0 \cos 2\theta$ and yields, in combination with $\eta(\theta)$ given in eq 4b, a θ- and ω-independent expression for the quadrupole splitting

$$\Delta E_Q = \frac{1}{2}eQV_{zz}\sqrt{1+\frac{1}{3}\eta^2} = \frac{1}{2}eQV_{zz}^0 \qquad (8)$$

in accordance with the aforementioned DFT results and the striking constancy observed for this quantity in Mössbauer studies of complexes with different symmetries: ΔE_Q (at 4.2 K) is -3.34 mm/s in $[Fe(S_2\text{-}o\text{-xyl})_4]^{2-}$ (D_{2d}), -3.24 mm/s in *Cp* Rd_{red} (C_2'), -3.25 mm/s in $[Fe(SPh)_4]^{2-}$ (C_2'), and -3.24 mm/s in $[Fe(SCH_2CH_3)_4]^{2-}$ (structure not reported).

Table 3. DFT-Calculated ΔE_Q Values for *Cp* Rd_{red} and $[Fe(SPh)_4]^{2-}$

	Cp Rd_{red}				$[Fe(SPh)_4]^{2-}$			
method	I[a]	II[b]	III[c]	exp	I[a]	II[b]	III[c]	exp
ΔE_Q[d] mm/s	−3.95	−3.48	−3.52	−3.25	−3.88	−3.44	−3.46	−3.24
η	0.79	0.81	0.78	0.75	0.96	0.98	0.90	0.67

[a] I: B3LYP/6-311G. [b] II: B3LYP/Wachters (+f), 6-311G. [c] III: B3LYP/6-311+G*. [d] Using conversion factor -1.72 mm s^{-1}/au based on nuclear quadrupole moment $Q = 0.17$ b.

The small variations in ΔE_Q along this series are probably caused by differences in the electron-withdrawing capabilities of the ligands in these complexes. The applicability of the valence-only expressions suggests that the ligand contributions to the EFG are small. This proposal was computationally tested by substituting Fe^{2+} in the $[Fe(SCH_3)_4]^{2-}$ model with Zn^{2+} (d^{10}), by which the valence contribution was eliminated while retaining the ligand contribution and confirmed by the smallness of the following result: $\Delta E_Q \approx 0.2$ mm/s at the Zn nucleus. (We used, for the sake of comparison, the conversion factor based on the nuclear moment of iron to convert the EFG at the Zn nucleus into mm/s.) The DFT values for ΔE_Q (Table 3), obtained for the model system $[Fe(SCH_3)_4]^{2-}$ with angles and distances taken from the X-ray structures (see Table 2), are slightly basis-set dependent and approach the experimental numbers for the *Cp* Rd_{red} and $[Fe(SPh)_4]^{2-}$ upon increasing the basis with polarization and diffuse functions. The results pertaining to the largest basis set employed are about 0.25 mm/s lower in value than those observed. The DFT values for η have also been listed and are in good agreement with the experiment, especially those calculated for the $[Fe(SCH_3)_4]^{2-}$ models in which the methyls represent alkyls.

In decreasing order of magnitude, the zero-field parameter D includes contributions arising from (i) the spin−orbit coupling between the crystal-field-split spin-quintet states (D_Q) of ^5D parentage, (ii) spin−orbit coupling of the quintet ground state with excited triplet states (D_T), and (iii) spin−spin coupling between the unpaired 3d electrons (D_{ss}). These quantities are additive in the second-order perturbation treatment adopted here:

$$D = D_Q + D_T + D_{ss} \qquad (9)$$

The relative magnitudes of the terms in eq 9 have been listed in Table 4 for three complexes. The expression for D_Q depends on the orbital function of the quintet ground state[31]

$$D_Q(z^2) = \frac{3\zeta^2}{16\epsilon_{xz,yz}} \qquad (10a)$$

$$D_Q(x^2-y^2) = -\frac{\zeta^2}{16}\left(\frac{4}{\epsilon_{xy}} - \frac{1}{\epsilon_{xz,yz}}\right) \qquad (10b)$$

where the doubly occupied orbital is indicated in parentheses. The first expression contains one term less than the second one because the z^2 ground state does not interact with the xy excited state by spin−orbit coupling. In the special case that the 3d orbitals of t_2 parentage are degenerate, $\epsilon_{xy} \approx \epsilon_{yz} \approx$

Table 4. Compositions of Zero-Field Splittings

system	D cm^{-1}	D_Q %	D_T %	D_{ss} %[a]	β-HOMO	ζ/ζ_{free}[b]	ref
Rd_{red}	5.7	51[c]	42[c]	7	$c\|z^2\rangle+s\|x^2-y^2\rangle$	0.89	this paper
$[Fe(SPh)_4]^{2-}$	5.7[d]	53[e]	0	47[f]	$c\|z^2\rangle+s\|x^2-y^2\rangle$	0.80	21
$[Fe(SPhC_6H_4)_4]^{2-}$	−8.7[g]	81[e]	14[g]	5[h]	$\|x^2-y^2\rangle$	0.91	11
	−8.7	70.5[i]	25[j]	4.5	$\|x^2-y^2\rangle$	0.85[k]	

[a] $D_{ss} = 3\rho = 0.54$ cm^{-1}, ρ is spin−spin coupling for free Fe^{2+} given by Watson and Blume.[37] [b] ζ used for scaling $D(\zeta_{free})$ to D_{exp} observed. $\zeta_{free} = 400$ cm^{-1}. [c] Calculated on the basis of d−d excitation energies deduced from TD-DFT. [d] From far-infrared studies by Champion and Sievers.[20] [e] Calculated on the basis of d−d excitation energies inferred from spectroscopic data. [f] Based on the spin−spin coupling constant estimated by Pryce,[35] $\rho = 0.95$ cm^{-1}. [g] From MCD. [h] Not considered by Gebhard et al.[11] [i] Percentage based on the value for D_Q given in Gebhard et al.[11] [j] Calculated with same excitation energies as used for D_T in Rd_{red} in the case of an $x^2 - y^2$ ground state. [k] Use of a larger value for D_T requires a smaller reduction factor to match D observed.

ϵ_{xz}, eq 10a,b implies the relation $D_Q(x^2 - y^2) \approx -D_Q(z^2)$. However, the DFT calculations, discussed below, indicate that $\epsilon_{xy} < \epsilon_{yz} \approx \epsilon_{xz}$. Substitution of the typical values $\epsilon_{xy} = 2400$ cm^{-1} and $\epsilon_{yz} \approx \epsilon_{xz} = 6000$ cm^{-1} in eq 10a,b yields the modified relation $D_Q(x^2 - y^2) \approx -3D_Q(z^2)$, which rationalizes both the negative sign and the increased size of the ZFS in the third complex of Table 4. However, the increase is less than predicted and indicates the presence of contributions other than D_Q that are less affected by the change of the orbital ground state. Using the free ion value $\zeta_{free} = 400$ cm^{-1}, one obtains the value $D_Q(z^2) = 5$ cm^{-1}, which is slightly below the experimental value for Rd_{red}. The large value of D_{ss} reported by Knapp et al.[21] (Table 4) is based on the spin−spin coupling constant estimated by Pryce[35] ($\rho = 0.95$ cm^{-1}) from deviations from the Landé rule, observed in the spectroscopic level spacings of the free Fe^{2+} ion. This estimate was challenged by Trees,[36] who realized that such deviations may also arise from off-diagonal spin−orbit coupling between the $2J + 1$ manifolds of the ion. After subtracting the latter effect, this author obtained spin−spin coupling constants ($\rho \sim 0.10$ cm^{-1}) considerably smaller than Pryce's estimates for this quantity, although it turned out to be difficult to determine precise values for ρ. The order of magnitude of ρ suggested by Trees was confirmed by the atomic Hartree−Fock calculations conducted by Watson and Blume, and we have adopted their theoretical estimate for this quantity,[37] $^1/_3D_{ss} = \rho = 0.18$ cm^{-1}. This value, the ζ_{free}-based value $D_T = 1.5$ cm^{-1} given by Gebhard et al.[11] (the sign of D_T is discussed below), and $D_Q = 5$ cm^{-1} (see above) yield together the estimate $D = 7$ cm^{-1} for the zero-field splitting in Rd_{red}. The latter D value is greater than the experimental result for Rd_{red} and suggests that ζ is covalently reduced to $0.9\zeta_{free}$ such that the ζ_{free}-based value for D scales down to the experimental value: $(\zeta/\zeta_{free})^2D(\zeta_{free}) \approx 5.7$ cm^{-1}. (We assume that D_{ss} scales as D_Q and D_T do.) However, if we adopt the reduction factor of Knapp et al.[21] ($\zeta = 0.8\zeta_{free}$) the scaled value for D (4.5 cm^{-1}) is smaller than observed, which would suggest that $D_T > 1.5$ cm^{-1}. These examples illustrate that there is some ambiguity in the estimates for the triplet contribution to the zero-field splitting. We have addressed this problem from a theoretical stand point, namely, by applying TD-DFT. The evaluation of D_Q and D_T requires the knowledge of the excitation energies, appearing in the denominators of the perturbation expressions, like those given in eq 10a,b. Table 5 presents excitation energies for the spin-quintet states and comprises the results of both computational (columns 2−4) and spectroscopic studies (column 6). The DFT calculations were performed on the model $[Fe(SCH_3)_4]^{2-}$ and were followed by TD-DFT computations of the excited states and their energies. Bond lengths and angles used for calculating columns 2 and 3 in Table 5 were taken to be equal to the corresponding values in the X-ray structure of Rd_{red}; those adopted in column 4 were acquired by a geometry optimization of the model in D_{2d} symmetry, and the results in column 5 were obtained with parameters in the D_{2d}-averaged X-ray structure of Rd_{red} (Table 2). The torsion angles of C_1 and C_3 in the structure of column 4 had to be artificially introduced after optimization because of the lack of any distorting protein strains in our structural model. The optimized structures are in good agreement with the X-ray structure and will be the subject of a future report. However, the differences between the X-ray-based and optimized structures had a significant impact on the excitation energies, especially on those for the *xz* and *yz* orbitals (Table 5), which were in fair agreement with experiment only after geometry optimization (compare to last column).

Table 5. d-d Excitation Energies for Quintet States and Orbital Energies Inferred from Triplet Energies

transition[a]	TDDFT[b] 6-311G X-ray[c]	TDDFT[b] 6-311+G* X-ray[c]	TDDFT[b] 6-311G C_2' $\omega = 20°$ [d]	triplets[b,e] 6-311G D_{2d}	exp $S = 2$
$\varphi \rightarrow (x^2 - y^2)$	3459[f]	3940	2741	2368	1000[g,h]
$\varphi \rightarrow xy$	3563	4424	2988	3441	2000[h,i]
$\varphi \rightarrow yz$	7737	8069	6343	7015	5900[j]
$\varphi \rightarrow xz$	9069	9261	7410	7015	6300[j]
B				682	620[k]
C				2583	2800[k]

[a] φ is β-HOMO. [b] Functional: B3LYP. Structure: $[Fe(SCH_3)_4]^{2-}$. [c] Angles and distances from structure of Rd_{red}.[6] [d] Angles and distances in $[Fe(SCH_3)_4]^{2-}$ from optimized D_{2d} structure. [e] Crystal-field energies and Racah parameters deduced from fitting TD-DFT triplet energies in D_{2d}. These values were used for the calculation of D_T and E_T. [f] Excitation energies and Racah parameters are expressed in wavenumbers. [g] Value fulfils condition >600 cm^{-1} obtained from the temperature dependence of ΔE_Q. [h] D_Q is not sensitive to these energies in Rd_{red}. [i] Value fulfils condition <3300 cm^{-1} obtained from MCD. [j] From MCD measurements.[14] [k] Inferred from single-crystal MCD measurements by Gebhard et al.[11] The free ion values are $B_{free} = 950$ cm^{-1} and $C_{free} = 3652$ cm^{-1}.[38]

The calculation of the triplet excitation energies is a complex matter, and we refer the reader to the Supporting Information for details of the treatment briefly described here. The $S = 2$ multiplet with two electrons in the orbital of eq 2 interacts by spin−orbit coupling with 26 strong-field spin-triplet states, which are listed in Table S1. These interactions

(35) Pryce, M. H. L. *Phys. Rev.* **1950**, *80*, 1107.
(36) Trees, R. E. *Phys. Rev.* **1951**, *82*, 683.
(37) Watson, R. E.; Blume, M. *Phys. Rev.* **1965**, *139*, 1209.

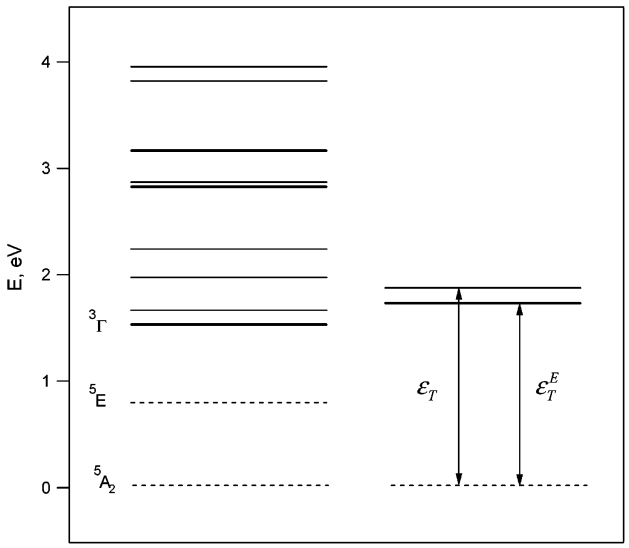

Figure 10. (Left) Theoretical energy level scheme of spin-quintet and -triplet d−d excited states that contribute to the ZFS in the ground state in D_{2d} symmetry. Triplet levels contributing to E_T terms linear in angle ω after distortion to C_2' symmetry are indicated by bold levels. (Right) Effective triplet energies defined in section 4.2.

contribute to the ZFS of the spin ground quintet of Rd_{red} (D_T and E_T). The excitation energies of the triplet states have been expressed in terms of Racah parameters, B and C (describing the electron−electron repulsions between the metal 3d electrons), and 3d-orbital energies ϵ_i (describing the crystal-field splittings of the metal 3d levels). These expressions are listed in Table S2. The energies of 12 of the 26 interacting triplets and those of three additional, noninteracting triplets were identified with the energies of TD-DFT solutions that were selected on the basis of their resemblance with the specified states. This procedure affords a total of nine excitation energies (Table S1). (The number of energies is lower than the number of states because of degeneracies, arising in the D_{2d} symmetry adopted in these calculations.) These energies were fitted with the theoretical expressions given in Table S2, using the Racah parameters and orbital energies as adjustable parameters (see Figure S.1). The optimized values are listed in Table 5 (column 5) and are in good agreement with the orbital energies obtained from the quintet calculations (column 4). The optimized parameters were substituted into the energy expressions for the crystal-field states (Table S2) of which we were not able to determine the energy by TD-DFT. The resulting triplet excitation energies together with those evaluated with the crystal-field expressions for the TD-DFT-identifiable states are listed in column 6 of Table S1 and were adopted in the calculation of zero-field splitting parameters, D_T and E_T. The theoretical level scheme of the states that interact by spin−orbit coupling with the largest orbital component (i.e., z^2) of the quintet ground state in Rd_{red} is shown in Figure 10. The lowest spin triplet is located ~1.5 eV above the ground state, in agreement with the MCD studies by Solomon and co-workers,[11] but is considerably lower in energy than the triplets computed by Bair and Goddard[22] ($E_{exc} > 2.8$ eV). The rather low triplet excitation energies obtained in our

Table 6. Calculated Quintet and Triplet Contributions to Zero-Field Parameters

	DFT-CFT[a]		CFT-MCD[b]	
	$\theta = 0°$	$\theta = -11.8°$	$\theta = 0°$	$\theta = -11.8°$
$D(^5A)$	4.36	3.63	4.92	3.92
$E/D(^5A)$	0	0.19	0	0.25
$D(^3\Gamma)$	3.30	3.04	3.19	2.91
$E/D(^3\Gamma)$	0	0.27	0	0.30
D_{ss}	0.54			
E_{ss}/D_{ss}	0	0.25	0	0.25
D	8.20	7.21	8.65	7.37
E/D	0	0.23	0	0.27
ζ reduction		89%		88%

[a] Energies taken from Table 5, columns 4 and 5; $\epsilon_{xz} = \epsilon_{yz} = 6877$ cm^{-1} in D_{2d}. [b] Energies taken from Table 5, column 6; $\epsilon_{xz} = \epsilon_{yz} = 6100$ cm^{-1} in D_{2d}.

calculations result from the small value for C, and it is therefore not surprising that our values for the Racah parameters are in excellent agreement with those inferred from the MCD data (see Table 5). Large reductions in B and C are expected for covalent ligands like sulfur. If the 3d components of the metal-based orbitals are diminished by orbital overlap with the ligands, $|d\rangle \rightarrow c|d\rangle$ ($c < 1$), the expectation values of the two-electron operators, $c^4(dd||dd)$, are reduced by factors that are the square of those for the one-electron operators, $c^2(d||d)$. Thus, the quantities $(C/C_{free})^{1/2} = 0.84$, $(B/B_{free})^{1/2} = 0.85$, and $\zeta/\zeta_{free} = 0.89$ are expected to be comparable in magnitude.[11,38] The ζ value (356 cm^{-1}) obtained by scaling D down to D_{exp} is in agreement with the result $\zeta \approx 350$ cm^{-1} deduced from the spin Hamiltonian parameters.

Substitution of the triplet energies (column 6 of Table S1) into the general expression for D_T (eq S3.13,14) results in the ζ_{free}-based values for this parameter listed in Table 6 (left). The right-hand side of Table 6 presents the results for D_T, obtained by adopting the experimental estimates of the quintet orbital excitation energies (column 6 of Table 5) as the orbital energies in the expressions for the triplet energies given in Table S2, while retaining the Racah parameters given in column 5 of Table 5. The replacement results in rather minor changes in D of less than 0.5 cm^{-1}. Furthermore, Table 6 lists D_Q values, which were calculated in second-order perturbation theory (eq 19.18 in ref 31) with the excitation energies in column 4 of Table 5 (Table 6, left) and with those in column 6 of Table 5 (Table 6, right). In the hypothetical case that all triplet energies are equal, $\epsilon_{^3\Gamma_i} = \epsilon_T$, the triplet contribution to D in the z^2 quintet ground state is given by

$$D_T \approx \frac{5}{16}\frac{\zeta^2}{\epsilon_T} \tag{11}$$

and has the same sign as the quintet contribution to D in this state (eq 10a). Equation 11 allows us to define an effective triplet energy, ϵ_T, by solving ϵ_T from eq 11; the value $D_T = 3.30$ cm^{-1}, given in Table 6, yields $\epsilon_T \approx 1.876$ eV (Figure 10, right). In passing we note that both D_Q and

(38) Ferguson, J.; Guggenheim, H. J.; Krausz, E. R. *Aust. J. Chem.* **1969**, *22*, 1809.

D_T obtained for the $x^2 - y^2$ quintet ground state have negative values and that $D_T(x^2 - y^2) \approx -D_T(z^2)$ for the same set of orbital energies. The theoretical value for $D_T(x^2 - y^2)$ can be accommodated in the D of $[Fe(S\text{-}2\text{-}(Ph)C_6H_4)_4]^{2-}$, provided ζ is reduced to $0.85\zeta_{free}$ (see Table 4).

Distortions from D_{2d} symmetry ($\omega = \theta = 0$) to C_2' ($0 < |\omega|, 2|\theta| < 180°$) give rise to (i) smaller values for D_Q and D_T in the z^2 quintet ground state and (ii) nonvanishing rhombicity parameters, E_Q and $E_T \neq 0$. The rhombicity parameters listed in Table 6 were evaluated at mixing angle $\theta = -11.8°$ in Rd_{red} with the electronic parameters used for calculating the corresponding D values, and are, in analogy with eq 9, additive quantities

$$E = E_Q + E_T + E_{ss} \tag{12}$$

The C_2' results for $D_Q(\theta)$ and $D_T(\theta)$ in Table 6 indicate that these functions have the maxima $D_Q(0)$ (eq 10a) and $D_T(0)$, respectively (eq 11). As a consequence, $D_Q(\theta) - D_Q(0) \sim \theta^2$ and $D_T(\theta) - D_T(0) \sim \theta^2$ so that D is altered insignificantly at small mixing angles θ. The percentages quoted in Table 4 for Rd_{red} are based on the C_2' results in Table 6 (left). In contrast to $D(\theta)$, the functions $E_Q(\theta)$ and $E_T(\theta)$ are approximately linear in θ. There are two factors contributing to the rhombicity parameter: (i) orbital mixing in the ground state (eq 2) and (ii) perturbations of the excited states, notably splittings of degenerate state energies by the C_2' distortions. For example, if the components of the ^3E states in D_{2d} (Table S1) are separated by an energy gap ($2\Delta\epsilon$) in C_2', there arise contributions to E_T of the form $\zeta^2/(\epsilon_T + \Delta\epsilon) - \zeta^2/(\epsilon_T - \Delta\epsilon) \sim D_T(\Delta\epsilon/\epsilon_T)$ leading to changes in E_T/D_T that are on the order of $\Delta\epsilon/\epsilon_T$. Given that $\Delta\epsilon$ is typically an orbital splitting energy caused by a small distortion ($\Delta\epsilon \sim 500$ cm^{-1}) and that $\epsilon_T \sim 2$ eV (see above), the changes in E_T/D_T are as little as ~2%. On the basis of this estimate, we have neglected any contributions to D_T and E_T that originate from excited-state modifications caused by torsion angle ω. The largest contribution to the rhombicity parameter in Rd_{red} arises from the admixture of $x^2 - y^2$ into the z^2 ground state. To analyze this ground-state effect on the ratio E/D, we have made first the simplifying assumptions that $\epsilon_{xz} = \epsilon_{yz}$ and that the triplet energies are degenerate, $\epsilon_{^3\Gamma_i} = \epsilon_T$. Under these conditions we obtain the expressions

$$\frac{E_Q}{D_Q} \approx \frac{E_T}{D_T} \approx \frac{\eta}{3} \tag{13}$$

that depend exclusively on the asymmetry parameter $\eta(\theta)$ (eq 4b) of the ground state. Equation 13 is independent of the excitation energies (which cancel by taking the ratios because E_T, $D_T \sim (\epsilon_T)^{-1}$ and D_Q, $E_Q \sim (\epsilon_{xz,yz})^{-1}$) and is also independent of the detailed form of the excited states because the closure relation in the second-order perturbation operator, $\sum_\Gamma(\epsilon_\Gamma)^{-1}|\Gamma\rangle\langle\Gamma| = (\epsilon_T)^{-1}\sum_\Gamma|\Gamma\rangle\langle\Gamma|$, is invariant under unitary transformation (i.e., orthogonality-conserving state mixing). The ratio of E (eq 12) and D (eq 9) can be written as

$$\frac{E}{D} = \frac{D_Q}{D}\left(\frac{E}{D}\right)_Q + \frac{D_T}{D}\left(\frac{E}{D}\right)_T + \frac{D_{ss}}{D}\left(\frac{E}{D}\right)_{ss} \approx \frac{\eta}{3} \tag{14}$$

where we have used eq 13 and $E_{ss}/D_{ss} \approx \eta/3$. Substitution of the asymmetry parameter for Rd_{red} in eq 14 yields $E/D \approx 0.25$, in excellent agreement with both the experiment and the values derived by a full calculation (Table 6). The latter result confirms the validity of the approximations made in the derivation of eq 14. It should be borne in mind, however, that the excited states that contribute to the ZFS parameters in eq 13 were assumed to be degenerate. In the expression for the quintet contribution (see eq 13), the assumed degeneracy is based on an idealized D_{2d} symmetry for the iron site in Rd (in which $\epsilon_{xz} \approx \epsilon_{yz}$); however, an analogous symmetry argument is lacking in the case of the triplet levels. The triplet states contributing to D_T and E_T belong to different sets (indicated by the bold levels in Figure 10), and therefore, the $(E/D)_T$ ratio in eq 13 is only an approximation. To derive a more accurate expression, it is convenient to define an effective energy, ϵ_T^E, for the triplet states that contribute to E_T linear terms in θ in the small angle approximation. A procedure, analogous to the one for evaluating ϵ_T, yields the effective energy, $\epsilon_T^E \approx 1.731$ eV (Figure 10, right). As $D_T \sim \epsilon_T^{-1}$ and $E_T \sim (\epsilon_T^E)^{-1}$, part of eq 13 has to be modified as follows:

$$\left(\frac{E}{D}\right)_T \approx \frac{\epsilon_T}{\epsilon_T^E}\frac{\eta}{3} \approx 0.36\eta \tag{15}$$

where the value 1.083 has been used for the ratio of the effective energies. This refinement leads to a slight modification of eq 14, $E/D \approx \eta/2.9$.

In summary, the rhombicities in fine structure and hyperfine interactions are related as

$$\frac{\eta}{3} \approx \frac{A_x^{sd} - A_y^{sd}}{3A_z^{sd}} \approx \left(\frac{E}{D}\right)_{ss} \approx \left(\frac{E}{D}\right)_Q \approx \left(\frac{E}{D}\right)_T \approx \frac{E}{D} \tag{16}$$

The asymmetry and rhombicity parameters for Rd_{red} (Table 1 and section 4.1) satisfy eq 16 within the error margins. The first two identities are generally true for orbitally nondegenerate high-spin Fe^{2+} and follow from the fact that the nuclear quadrupole interaction, the spin-dipolar coupling, and the ZFS because of spin−spin coupling are proportional to the same tensor (eq 19.15 in ref 31), whereas the last three identities are a peculiarity of the orbital ground state in Rd_{red} (Figure 8). The factor of $^1/_3$ in the first term of eq 16 is conventional and expresses that the maximum rhombicities (i.e., $\eta = 1$ and $E/D = {}^1/_3$) are attained (almost) simultaneously in each of the six terms in eq 16.

4.3. Whole Cells. The Mössbauer spectra of Rd_{red} in whole cells of *E. coli* have provided interesting information on Rd itself but also broader insights into the potential of whole-cell Mössbauer spectroscopy. We first wish to point out that one can obtain well-resolved spectra of Rd_{red} in whole cells (Figure 4B−E). The spectral components of Rd_{red} in the cellular spectra are virtually the same as those observed for the purified enzyme. This result suggests that the structure of the $[Fe(SR)_4]^{2-}$ unit in the cellular environment is the same as in frozen buffered solution. Even minute changes in some of the electronic parameters would have resulted in

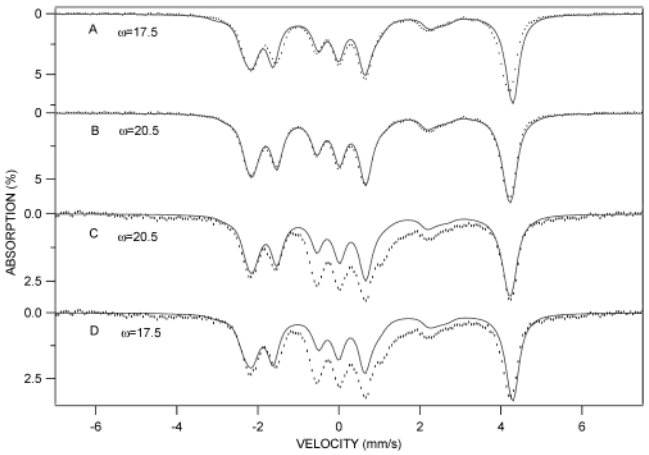

Figure 11. Effect of a small increment in the torsion angle, $\Delta\omega = 3°$, on the Mössbauer spectra of Rd_{red}. Experimental spectra A and B were obtained at 4.0 T for the as-isolated protein while spectra C and D were obtained for whole cells. A and D show theoretical spectra obtained from the best set (B and C) by changing ω by 3°. Parameters used are listed in section 4.3.

observable changes in the spectra. For instance, variations in ΔE_Q (1%), A_y (2%), δ (2%), D (10%), and E/D (15%) can be readily recognized. Of course, a structural distortion at the metal site will alter all spin Hamiltonian parameters simultaneously. The mixing parameter θ of eq 2 is related to the torsion angles ω_i of the S_i-C_β bonds (see above). To test the structure dependence of the spectra, the two torsion angles in Figure 6 (C_2' symmetry) have been rotated together, either clockwise or counterclockwise by an additional $\pm 3°$. As shown above, a distortion of $\Delta\omega \approx \pm 3°$ translates into $\Delta\theta \approx \pm 2°$ in the ground state of eq 2 and alters the spin Hamiltonian parameters in eqs 3−6. For example, for $\Delta\omega = -3°$ the relevant spin Hamiltonian parameters (and changes) are as follows: $D = 5.7$ (6.0) cm^{-1}, $E/D = 0.25$ (0.19), $\eta = 0.75$ (0.62), $A_x = -20.6$ (−19.8) MHz, $A_y = -11.4$ (−12.1) MHz, and $A_z = -32.8$ (−33.4) MHz. Figure 11 shows again the 4.0 T spectra obtained for the purified protein (spectra A and B) and for whole cells (spectra C and D) together with the simulations for the optimized parameter set (spectra B and C) and the changed set (spectra A and D): The simulations indicate that the change $\Delta\omega = 3°$ would be quite apparent. Thus, the similarity of the Rd_{red} components in the Mössbauer spectra of whole cells and purified protein samples indicates that the key features in the structure of the iron site are virtually the same in both environments.[39] The example of Rd_{red} illustrates that Mössbauer spectroscopy can provide precise and reliable structural information on the active site of iron-containing proteins within whole cells. It is noteworthy that a 1-mL sample cup packed with *E. coli* cells contains a fairly high concentration of iron (the sample of Figure 4B has ca. 120 μg of ^{57}Fe), and consequently, a Mössbauer spectrum with good signal/noise ratio can be collected within a few hours.

Rd_{red} is certainly a favorable case for whole-cell Mössbauer studies. Thus, the reduced protein has an isomer shift ($\delta = 0.70$ mm/s) that is distinctly different from those observed for 5- and 6-coordinated complexes with N and/or O ligands ($\delta \approx 1.1-1.3$ mm/s). Furthermore, the high-field spectra are well-resolved and reasonably sensitive to variations of the spin Hamiltonian parameters. Among the many proteins studied in our laboratory over the past 25 years, we can readily identify some, such as 3,4-protocatechuate dioxygenase and proteins containing reduced $[3Fe-4S]^0$ clusters that provide similar resolution. On the other hand, diferrous states of diiron proteins offer only a limited resolution in strong applied fields and, thus, structural information will not readily be obtainable. However, we have only just begun the systematic study of Mössbauer spectra from proteins in whole cells and foresee that it will be possible to reduce the spectral background absorption by making an appropriate choice of the growth conditions and timing of ^{57}Fe addition. Indeed, as shown here and in previous investigations,[23] the background ^{57}Fe absorption from cell components other than the protein of interest is a crucial point in several respects.

In our previous whole-cell study of the FNR transcription factor, as well as in other unpublished investigations, we have noticed that a considerable fraction of the Mössbauer absorption (at 4.2 K and in weak fields) of the various iron components in the cells consisted of a superposition of broadened quadrupole doublets, similar to that shown in Figure 5A. Lowering the temperature to ca. 1.5 K revealed that this absorption predominantly originated from paramagnetic species, mostly associated with high-spin ferric ions. (Low-spin ferric ions generally have larger quadrupole splittings than those observed in the spectrum of Figure 5A.) The observation of doublets at 4.2 K and spectra exhibiting paramagnetic hyperfine structure at 1.5 K indicates that the relaxation rates of the electronic spins are fast on the Mössbauer time scale at 4.2 K but are slow at 1.5 K. In our previous study of FNR transcription factor[23] we had speculated that some of the magnetic features were associated with the iron clusters of ferritin components. However, subsequent studies of *E. coli* mutants, lacking ferritin genes, showed that the absorption attributed to ferritin originated from other complexes.[23] The broad absorption features in the spectrum of Figure 5B most likely reflect a distribution of ferric species with different zero-field splittings. Since the magnetic hyperfine splittings of high-spin ferric ions depend sensitively on the parameter E/D, complexes with different E/D values will have splittings that differ by as much as a factor of 2.5; see eq 15 and Figure 4 of ref 40. Given that the magnetic hyperfine splittings are also a function of ΔE_Q and A_i, the broad spectral pattern observed is readily rationalized but nearly impossible to deconvolute. (N.B. The two lines in the center of the spectrum of Figure 5B do not represent a quadrupole doublet but originate from a superposition of the two central lines of a distribution of magnetically split 6-line patterns.)

(39) We have stated above that we would readily observe a 2% change in A_y, and the reader may wonder why we present an example where A_y increases by 6%. However, the change causes a change in D and E/D that yields a 2% smaller expectation value $\langle S_y \rangle$. Consequently, the critical quantity, the internal magnetic field, changes by only 4%.

(40) Münck, E. In *Physical Methods in Bioinorganic Chemistry*; Que, L., Jr., Ed.; University Science Books: Sausalito, CA, 2000; p 287.

The paramagnetism of the background ^{57}Fe absorption might be affected by interactions between closely spaced iron centers in whole cells. We have therefore attempted to assess this factor even though the intracellular volumes in the cell pellets, used to record the spectra of Figures 4 and 5, are not accurately known. A crude estimation suffices for the purpose of the present discussion: the intracellular volume is quite certainly within 20−80% of the total volume. Thus, if we adopt the value of 40%, the error will be at most 2-fold. With this choice of the volume ratio, the sample containing Rd-overproducing cells (Figure 4) and the control sample (Figure 5) would have intracellular iron concentrations of ca. 4 and 8 mM, respectively. From the spectra of Figure 4B−D, the intracellular Rd_{red} concentration can be estimated as 2.3 mM. If all molecules that contain paramagnetic iron centers (assuming mononuclear centers) were uniformly distributed in the cell, the average iron−iron distance would be about 60 Å at the highest estimated concentration (8 mM). The upper error limit given above for the volumes (2-fold) would translate into 1.25-fold (cubic root) distances. Thus, a conservative estimate of the average distance between the iron centers would be 40−75 Å. The spin−spin relaxation at these distances is expected to be slow, as it is indeed observed for the Rd_{red} component in the spectra. This raises the question of why, in contrast to Rd_{red}, the iron-containing species in the control of Figure 5 exhibit fast relaxation at 4.2 K. A possible explanation may be that the paramagnetic sites in these species are not uniformly distributed in the cell and are separated by subaverage intermolecular distances. Moreover, as these species are predominantly high-spin ferric they may effectively relax with non-iron paramagnetic centers, such as Mn(II) or other metals.

Finally, the effect of paramagnetic cell constituents on the spectra of the protein of interest appears to be negligible in the case of Rd_{red}. Investigations on other well-characterized proteins are in progress to determine whether this is a general occurrence. It would then be possible to infer that whole-cell spectra reflect genuine structural features of the protein of interest, regardless of the magnetic properties of the cellular medium.

The present investigation has disclosed another fact that is at the same time a weakness and a strength of the technique. The spectra of Figure 4B−D show that Rd in whole cells is only present in its reduced state, Rd_{red}. This is readily understood by taking into account that the intracellular chemical potential (−260 to −280 mV)[41] is much lower than the redox potential of Rd (−60 to −90 mV). Hence, in some cases it may only be possible to probe one redox level of a given active site by whole-cell Mössbauer spectroscopy. However, this consideration also suggests that the method could be used for monitoring the chemical potential of cells. Preliminary studies using [2Fe−2S] ferredoxins look promising, although the question of the intracellular redox pools with which the ferredoxins equilibrate must be answered. Moreover, it has to be tested whether the cell potential shifts during concentration of cells by centrifugation and subsequent freezing. Investigations along these lines are in progress by using a series of iron−sulfur proteins that span an appropriate range of redox potentials.

Acknowledgment. This work was supported by National Institutes of Health Grant GM 22701 (E.M.).

Supporting Information Available: Triplet excitations and their contributions to the zero-field splitting. This material is available free of charge via the Internet at http://pubs.acs.org.

IC020508Y

(41) Ritz, D.; Beckwith, J. *Annu. Rev. Microbiol.* **2001**, *55*, 21.